

Hydrothermal synthesis, crystal structures, and properties of Co^{II} and Ni^{II} supramolecular complexes with 2,4,6-trimethyl benzoate and 4,4'-bipyridyl

Murugan Indrani^{a,*}, Ramasamy Ramasubramanian^a, Sudalaiandi Kumaresan^a, Sung Kwon Kang^b, Min Chen^c, Miao Du^c

^a Department of Chemistry, Manonmaniam Sundaranar University, Tirunelveli 627 012, Tamil Nadu, India

^b Department of Chemistry, Chungnam National University, Daejeon 305-764, South Korea

^c College of Chemistry and Life Science, Tianjin Normal University, Tianjin 300387, PR China

ARTICLE INFO

Article history:

Received 17 May 2008

Accepted 8 September 2008

Available online 22 October 2008

Keywords:

Co^{II} and Ni^{II} complexes

2,4,6-Trimethylbenzoate

4,4'-Bipyridyl

Hydrogen bonding, structures and properties

ABSTRACT

Two new coordination complexes, viz. [Co(tmb)₂(4,4'-bpy)₂(H₂O)₂](Htmb)₂ (**1**) and {[Ni(tmb)₂(μ-4,4'-bpy)₂(H₂O)₂}(4,4'-bpy)_n (**2**), have been hydrothermally synthesized by reaction of the corresponding metal acetate with 2,4,6-trimethylbenzoic acid (Htmb) and 4,4'-bipyridyl (4,4'-bpy). X-ray single-crystal diffraction suggests that complex **1** represents a discrete mononuclear species in which the central metal ion is coordinated by the terminal carboxylate moiety and the 4,4'-bipyridyl ligand. The crystal structure of complex **2** reveals a 1D chain coordination polymer in which the Ni(II) ions are connected by the bridging 4,4'-bipyridyl ligands. In both cases, the coordination arrays are further extended via hydrogen bonding interactions to generate 3D supramolecular networks. Complexes **1** and **2** have also been characterized by spectroscopic (IR and UV/Vis), thermal (TGA) and magnetic susceptibility measurements. In addition, both complexes exhibit antimicrobial activity.

© 2008 Elsevier Ltd. All rights reserved.

1. Introduction

Recently, supramolecular coordination complexes with diverse organic bridging ligands have attracted extensive attention because they not only possess potential applications in catalysis, magnetism, optical material and adsorption [1–4], but also display intriguing architectures in virtue of coordination and/or secondary interactions. Till now, a number of complexes containing transition metal ions and bridging multi-functional ligands with N- and O-donors have been reported [5].

Ligands with particular symmetry and stereochemistry may lead to the formation of various specific architectures. For example, exo-bidentate building blocks such as 4,4'-bipyridyl (4,4'-bpy), pyrazine, 1,2-bis-(4-pyridyl)ethylene, and 1,2-bis(4-pyridyl)ethane, have widely been used for constructing polymeric chains [6,7]. Focusing only on 4,4'-bipyridyl as ligand, a survey of the recent literature reveals a number of homopolymetallic complexes with interesting supramolecular architectures [8–11]. This ligand is an ideal connector between the transition metal ions for the propagation of coordination networks due to the following features: it has two potential binding sites which are arranged in a divergent (exo) fashion; it has a rigid backbone which will help in

the predictability of network geometries; the length of the ligand is suitable to create the cavities of molecular dimensions upon the formation of networks with metal ions. In principle, the pyridyl groups of 4,4'-bipyridyl can rotate along the central C–C bond, which, however, does not affect the mutual orientation of the two terminal lone pairs. Therefore, it can be regarded as a rigid and prototypical bridging ligand. Curiously enough, 4,4'-bipyridyl has been shown to form a variety of coordination networks ranging from 1D to 3D with the familiar transition metal salts. The resultant framework architectures depend on several factors such as coordination geometry of the metal ion, counter anions, guest molecules, and the ligand/metal ratio used in the reaction etc. [12].

Although 4,4'-bipyridyl has been extensively used for constructing numerous types of compounds [13], the employ of 2,4,6-trimethylbenzoic acid (Htmb) in crystallographic investigation appears to be scarce [14]. In this work, we will present the hydrothermal synthesis and crystal structures of two new Co^{II} and Ni^{II} supramolecular complexes assembled from 4,4'-bipyridyl in conjunction with such a aromatic carboxylate species as the anionic co-ligand. The 4,4'-bipyridyl component may serve as both terminal and bridging building block in the complexes, and the discrete or 1D coordination entities can be extended to interesting 3D hydrogen-bonding architectures. The thermal, magnetic and antimicrobial properties of the complexes have also been investigated.

* Corresponding author.

E-mail address: indrani_dec14@yahoo.co.in (M. Indrani).

2. Experimental

2.1. General consideration

All starting materials were obtained commercially from Aldrich. IR spectra were recorded on a JASCO FTIR-410 spectrometer using KBr pellets. UV/Vis spectra were recorded on a Perkin-Elmer Lambda25 UV/Vis spectrophotometer. Thermogravimetric analysis was performed on a Mettler Toledo Star system from room temperature to 700 °C with a heating rate of 10 °C/min. Elemental analysis was carried out using a Perkin-Elmer 1400 C analyzer. Magnetic susceptibility measurements were performed on a George Associates Faraday Force Magnetometer.

2.2. Preparation of $[\text{Co}(\text{tmb})_2(4,4'\text{-bpy})_2(\text{H}_2\text{O})_2](\text{Htmb})_2$ (**1**)

A mixture of cobalt acetate tetrahydrate (0.0311 g, 0.125 mmol), Htmb (0.041 g, 0.250 mmol), 4,4'-bpy (0.039 g, 0.250 mmol) and water (2.5 mL) was stirred for 30 min, sealed in a 23 mL polyfluoroethylene-lined stainless steel bomb, and kept at 100 °C under autogenous pressure for 72 h. After cooling at a ramp of 10 °C/h to room temperature, pink colored crystals of **1** were collected by filtration, washed with deionized water followed by diethyl ether, and then dried (0.0858 g, 65% yield).

For **1**: Anal. Calc. for $\text{C}_{60}\text{H}_{66}\text{N}_4\text{O}_{10}\text{Co}$: C, 67.85; H, 6.26; N, 5.28. Found: C, 68.25; H, 6.02; N, 5.60%.

2.3. Preparation of $\{[\text{Ni}(\text{tmb})_2(\mu\text{-}4,4'\text{-bpy})_2(\text{H}_2\text{O})_2](4,4'\text{-bpy})\}_n$ (**2**)

A mixture of nickel acetate tetrahydrate (0.0311 g, 0.125 mmol), Htmb (0.041 g, 0.250 mmol), 4,4'-bpy (0.039 g, 0.250 mmol) and water (2.5 mL) was stirred for 30 min, sealed in a 23 mL polyfluoroethylene-lined stainless steel bomb, and kept at 75 °C under autogenous pressure for 72 h. After cooling at a ramp of 10 °C/h to room temperature, green colored crystals of **2** were collected by filtration, washed with de-ionized water followed by diethyl ether, and then dried (0.0641 g, 70% yield).

For **2**: Anal. Calc. for $\text{C}_{40}\text{H}_{42}\text{N}_4\text{O}_6\text{Ni}$: C, 65.50; H, 5.77; N, 7.64. Found: C, 66.23; H, 5.49; N, 7.51%.

2.4. X-ray data collection and structure refinement of **1** and **2**

X-ray single-crystal diffraction data for compound **1** was collected on a CAD-4 diffractometer equipped with graphite monochromated Mo K α radiation at 293 K. The data was collected by the $\omega/2\theta$ scan mode. The standard direct method was used to position the heavy atoms. The remaining non-H atoms were located from the subsequent difference Fourier synthesis. All non-H atoms were refined anisotropically. All H atoms were calculated in ideal positions and were riding on their respective carbon atoms (Biso = 1.2 Beq and 1.5 Beq). The structure was refined in a full matrix least-squares calculation on F^2 . Programs used to solve and refine the structure: SHELXS97 and SHELXL97 [15]. Molecular graphics: ORTEP-3 for windows [16].

X-ray single-crystal diffraction data for compound **2** was collected on a Bruker Apex II CCD diffractometer at 293(2) K. A semi-empirical absorption correction was applied using SADABS [17] and the SAINT program [18] was utilized for integration of the diffraction profiles. The structure was solved by direct methods using the SHELXS program of the SHELXTL package [19] and refined with SHELXL. The final refinement was implemented by full-matrix least-squares methods on F^2 with anisotropic thermal parameters for all the non-H atoms. In general, H atoms attached to the ligands were placed geometrically and allowed to ride during the subsequent refinement. The crystal data for both complexes are

presented in Table 1, and selected bond distances and angles are in Tables 2 and 3.

3. Results and discussion

3.1. Structural description of $[\text{Co}(\text{tmb})_2(4,4'\text{-bpy})_2(\text{H}_2\text{O})_2](\text{Htmb})_2$

Compound **1** crystallizes in the monoclinic space group $P2_1/n$. The cobalt center locates on the inversion center and coordinates to two nitrogen atoms from two 4,4'-bipyridyl, two oxygen atoms from two 2,4,6-trimethylbenzoate groups, and two oxygen atoms from a pair of water molecules to form an octahedral geometry. In this complex, there exist two unique 2,4,6-trimethylbenzoic acid moieties (see Fig. 1), one in anionic form to constitute the $[\text{Co}(\text{tmb})_2(4,4'\text{-bpy})_2(\text{H}_2\text{O})_2]$ monomer via coordination with car-

Table 1
Crystal data and structure refinement for **1** and **2**

Complex	1	2
Empirical formula	$\text{C}_{60}\text{H}_{66}\text{N}_4\text{O}_{10}\text{Co}$	$\text{C}_{40}\text{H}_{42}\text{N}_4\text{O}_6\text{Ni}$
Formula weight	1062.1	733.49
Temperature (K)	293(2)	294(2)
Wavelength (Å)	0.71073	0.71073
Crystal system	monoclinic	orthorhombic
Space group	$P2_1/n1$	$Ccca$
Unit cell dimensions		
<i>a</i> (Å)	10.4363(8)	12.992(2)
<i>b</i> (Å)	13.0223(9)	26.101(4)
<i>c</i> (Å)	20.6962(12)	22.618(4)
<i>V</i> (Å ³)	2812.0(3)	7670(2)
<i>Z</i>	2	8
<i>D</i> _{calc} (mg m ⁻³)	1.254	1.270
Absorption coefficient (mm ⁻¹)	0.366	0.556
<i>F</i> (000)	1122	3088
Crystal size (mm)	0.38 × 0.28 × 0.23	0.40 × 0.32 × 0.20
θ Range for data collection (°)	1.85–28.31	1.56–27.85
Limiting indices	–13 ≤ <i>h</i> ≤ 13 –17 ≤ <i>k</i> ≤ 17 –27 ≤ <i>l</i> ≤ 26	–17 ≤ <i>h</i> ≤ 16 –33 ≤ <i>k</i> ≤ 32 –21 ≤ <i>l</i> ≤ 29
Reflections collected/unique	30218/6982	22765/4564
<i>R</i> _{int}	0.0474	0.0336
Completeness to θ (%)	100.0	100.0
Absorption correction	none	none
Refinement method	full-matrix least-squares on F^2	
Data/restraints/parameters	6982/0/357	4564/0/236
Goodness-of-fit on F^2	1.017	1.025
<i>R</i> ₁ and <i>wR</i> ₂ [<i>I</i> > 2 σ (<i>I</i>)]	0.0479, 0.1148	0.0354, 0.0878
<i>R</i> ₁ and <i>wR</i> ₂ (all data)	0.0828, 0.1340	0.0629, 0.1016
Largest difference in peak and hole (e Å ⁻³)	0.541 and –0.350	0.278 and –0.326

Table 2
Selected bond lengths (Å) and angles (°) for **1**

Co–O(1)#1	2.0749(16)	C(10)–N(11)	1.318(4)
Co–O(1)	2.0749(16)	C(20)–O(21)	1.248(3)
Co–O(21)#1	2.1338(14)	C(20)–O(22)	1.261(3)
Co–O(21)	2.1338(14)	C(32)–O(34)	1.194(3)
Co–N(2)#1	2.1787(16)	C(32)–O(33)	1.306(3)
Co–N(2)	2.1787(16)	O(33)–H(33)	0.9300(4)
O(1)#1–Co–O(1)	180.00(11)	O(21)–Co–N(2)	88.19(6)
O(1)#1–Co–O(21)	93.25(6)	O(21)#1–Co–N(2)	91.81(6)
O(1)–Co–O(21)	86.75(6)	O(1)#1–Co–N(2)#1	90.66(6)
O(1)#1–Co–O(21)#1	86.75(6)	O(1)–Co–N(2)#1	89.34(6)
O(1)–Co–O(21)#1	93.25(6)	O(21)–Co–N(2)#1	91.81(6)
O(21)–Co–O(21)#1	180.00(11)	O(21)#1–Co–N(2)#1	88.19(6)
O(1)#1–Co–N(2)	89.34(6)	N(2)–Co–N(2)#1	180.00(12)
O(34)–C(32)–O(33)	122.3(3)	O(1)–Co–N(2)	90.66(6)
O(21)–C(20)–O(22)	123.6(2)		

Symmetry transformation used to generate equivalent atoms: #1 –*x* + 1, –*y*, –*z*.

Table 3
Selected bond lengths (Å) and angles (°) for **2**

Ni(1)–O(1)	2.0419(14)	Ni(1)–N(2)#2	2.105(2)
Ni(1)–O(1)#1	2.0419(14)	O(1)–C(7)	1.259(2)
Ni(1)–O(3)	2.0835(13)	O(2)–C(7)	1.248(2)
Ni(1)–O(3)#1	2.0835(13)	N(2)–Ni(1)#3	2.105(2)
Ni(1)–N(1)	2.1041(18)		
O(1)–Ni(1)–O(1)#1	177.04(7)	O(1)#1–Ni(1)–N(1)	88.52(3)
O(1)–Ni(1)–O(3)	90.39(5)	O(3)–Ni(1)–N(1)	88.77(3)
O(1)#1–Ni(1)–O(3)	89.54(5)	O(3)#1–Ni(1)–N(1)	88.77(3)
O(1)–Ni(1)–O(3)#1	89.54(5)	O(1)–Ni(1)–N(2)#2	91.48(3)
O(1)#1–Ni(1)–O(3)#1	90.39(5)	O(1)#1–Ni(1)–N(2)#2	91.48(3)
O(3)–Ni(1)–O(3)#1	177.55(7)	O(3)–Ni(1)–N(2)#2	91.23(3)
O(1)–Ni(1)–N(1)	88.52(3)	O(2)–C(7)–O(1)	125.32(18)

Symmetry transformations used to generate equivalent atoms: #1 $-x + 1/2, -y, -z$; #2 $x, -y, z - 1/2$; #3 $x, -y, z + 1/2$.

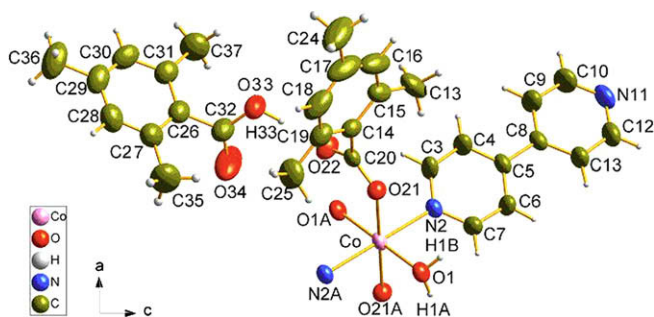


Fig. 1. A portion view of **1** with atom labeling of the asymmetry unit and metal coordination sphere. Symmetry code (A) $-x + 1, -y, -z$.

boxylate and the other in the free acid form that is involved in hydrogen bonding linkage.

The bond lengths involving 4,4'-bipyridyl and 2,4,6-trimethyl benzoate ligands, Co(1)–N(2) [2.1787(16) Å], Co(1)–O(1) [2.0749(16) Å] and Co(1)–O(21) [2.1338(14) Å], are comparable to those found in similar cobalt complexes [20]. The *cis*-O–Co–O/N angles are in the range of 86.75(6)–91.81(6°) and the O–C–O angle is 123.6(2°).

Due to the trans-disposition of the aqua molecules and both types of organic ligands at each metal center, a square grid layer network is propagated along the crystallographic *bc* plane with the adjacent Co–Co distance of 13.022 Å via intermolecular O–H...N interactions, as shown in Fig. 2 [21]. The bridging role of 4,4'-bipyridyl ligand via both coordination and H-bonded contacts leads to the formation of a (4,4) sheet, in which the ligated 2,4,6-trimethyl benzoate moieties lie along the shorter diagonals within each subunit and the unligated 2,4,6-trimethyl benzoic acid molecules recline the length of the longer diagonal by virtue of hydrogen bonds (Scheme 1).

In detail, the water ligands form strong intermolecular hydrogen bonds to the uncoordinating carboxylate oxygen atoms with $d_{O1-H1A...O22} (-x + 1, -y, -z) = 2.660(2)$ Å and $\angle = 158(3)$, and also to the uncoordinating N atoms of 4,4'-bipyridyl, with $d_{O1-H1B...N11} (-x + 3/2, y + 1/2, -z + 1/2) = 2.767(3)$ Å and $\angle = 179(4)$. In addition, there exist strong hydrogen bonds between the 2,4,6-trimethyl benzoic acid guests and the unligated O atoms of the 2,4,6-trimethyl benzoate ligands with $d_{O33-H33...O22} = 2.586(3)$ Å and $\angle = 175(4)$.

Also, there are C–H...O interactions present in the structure [$d_{C36-H36B...O21} (x + 1/2, -y + 1/2, z - 1/2) = 3.594(4)$ Å and $\angle = 163.86(2)$], [$d_{C10-H10...O34} (x + 1/2, -y - 1/2, z + 1/2) = 3.333(4)$ Å and $\angle = 154.77(20)$], [$d_{C7-H7...O34} (-x + 1, -y, -z) = 3.630(4)$ Å and $\angle = 152.04(15)$], and [$d_{C3-H3...O22} = 3.721(3)$ Å and $\angle = 143.81(16)$], which play a significant role in stabilizing the overall 3D structure (see Fig. 3). The parameters of hydrogen bonds are given in Table 4.

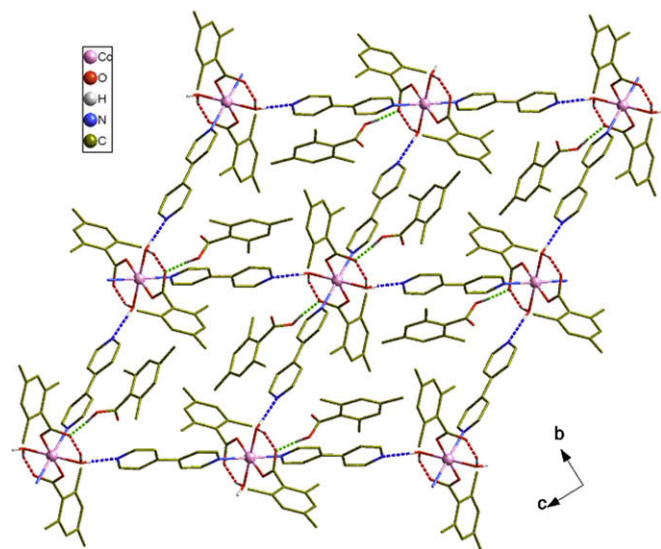


Fig. 2. A perspective view of the 2D H-bonding layer in **1** along the [100] direction. (H-bonds are shown in red, blue, and green broken lines). (For interpretation of the references to colour in this figure legend, the reader is referred to the web version of this article.)

From the least square plane calculations, the phenyl rings of two 2,4,6-trimethylbenzoate anions and the two 4,4'-bipyridyl ligands are located in the parallel planes and separated by the distances of 1.914 and 0.264 Å, respectively.

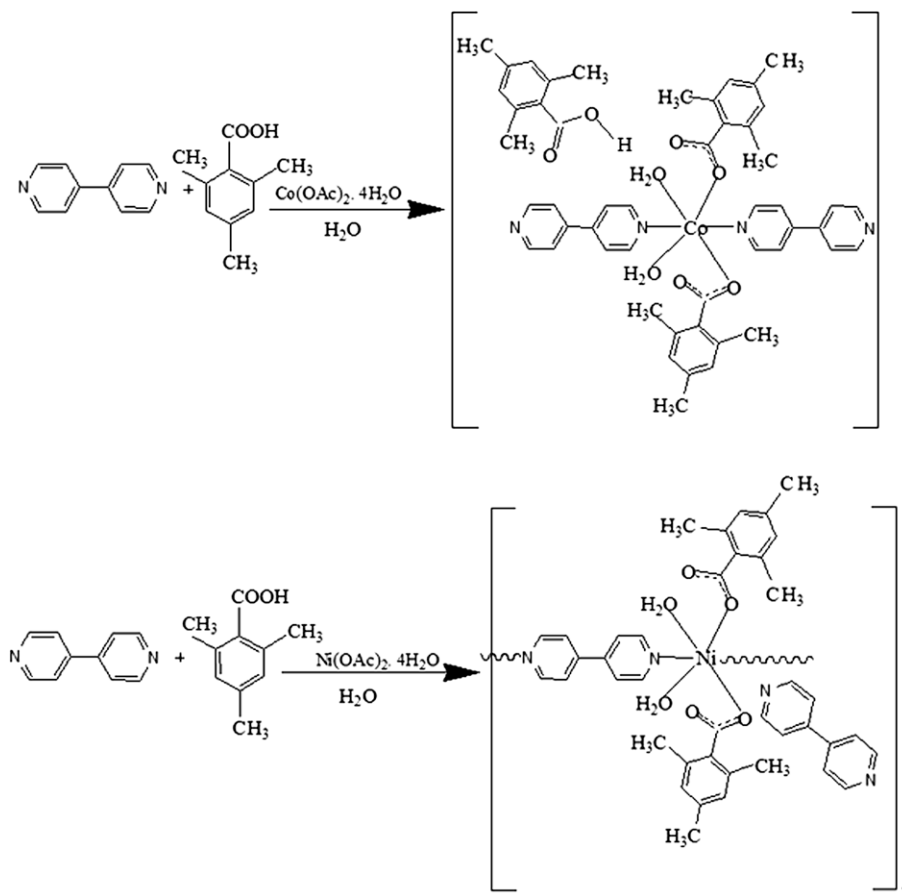
The dihedral angle between the 4,4'-bipyridyl ring and a phenyl ring of 2,4,6-trimethyl benzoate anion is 63.79° for the planes containing (C14, C15, C16, C17, C18, and C19) and (N2, C3–C10, N11, C12, and C13), and the dihedral angle between the phenyl rings of coordinated and uncoordinated acids is 63.20° for the planes containing (C14, C15, C16, C17, C18, and C19) and (C26, C27, C28, C29, C30, and C31) [22].

The group of atoms (N2, C3–C10, N11, C12, and C13) in the 4,4'-bipyridyl unit deviate significantly from planarity. Among all, C4 has the highest deviation of 0.0877 Å. The group of atoms (C14–C20 and C23–C25) of the trimethyl benzoate moiety also deviate significantly from planarity and C24 has the highest deviation of 0.1668 Å.

The group of atoms (C20, O21, and O22) in the carboxylate moiety are coplanar but, almost perpendicular (dihedral angle 88.84°) to its phenyl ring (C14–C19). The group of atoms (C26–C32 and C35–C37) deviates significantly from planarity, and C32 has the higher deviation of 0.0182 Å. From the puckering parameters (φ_2 , θ_2 , and Q) [23,24] the conformation for ring 1 (C14–C19) is boat conformation 1,4B , for ring 2 (C26–C31) is twist conformation 4T_2 , for ring 3 (N2 and C3–C7) is twist conformation 3T_1 , and for ring 4 (C8–C9, N11, C12, and C13) is sofa conformation 3S_4 .

3.2. Structural description of $\{[Ni(tmb)_2(\mu-4,4'-bpy)(H_2O)_2](4,4'-bpy)_n\}$

Compound **2** crystallizes in the orthorhombic space group *Ccca*. It is a 1:1:2 complex with Ni ion, 2,4,6-trimethylbenzoic acid (Htmb), and 4,4'-bipyridyl. The Ni atom lies on a diad axis and has a *trans*- N_2O_4 octahedral coordination through bonds to two 4,4'-bpy N atoms, two equivalent water O atoms and two equivalent carboxylate–O atoms. In the asymmetric unit, both COOH group of Htmb and 4,4'-bpy interact with Ni(II). Thus, each Ni(II) is connected to two 4,4'-bpy molecules that lie at the axial positions and two Htmb to complete the six coordination sites with the aid of two water molecules (Fig. 4). As a result, in this case, infinite linear polymeric chains of $-Ni-bpy-Ni-bpy-$ are formed



Scheme 1.

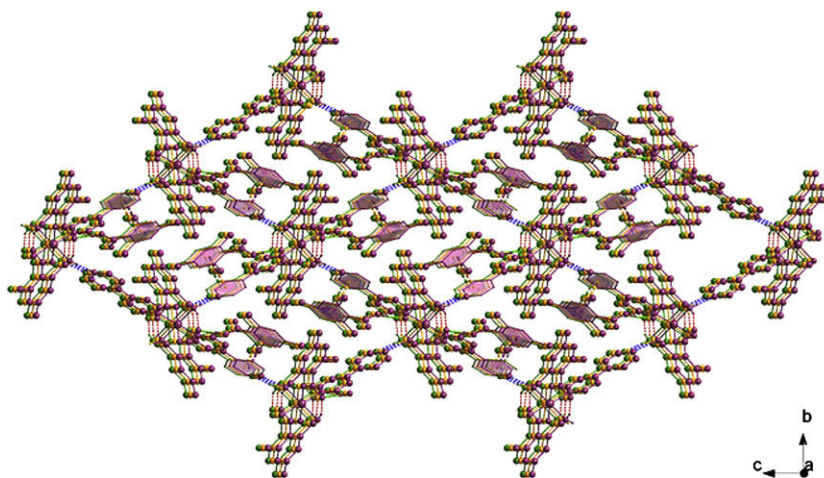


Fig. 3. 3D packing diagram of **1**, in which the interlayer aromatic interactions are indicated by pink. (For interpretation of the references to colour in this figure legend, the reader is referred to the web version of this article.)

running parallel to the *c*-axis by repeated operations of *c*-glide (see Fig. 5), with the 4,4'-bpy connectors joining the adjacent Ni^{II} octahedrons using their typical bridging role. In each chain, the basal plane of carboxylate and water O atoms is stabilized by O3–H···O2 hydrogen bonding from water to the uncoordinated carboxylate O.

These polymeric chains are further held together by O3–H···N(bpy)N···H–O3 bridges. In short, there is much symmetry including glide planes and 2-fold rotation axes in all three direc-

tions, 2-fold screw axes in two directions, inversion centers, and lattice centering in this structure.

In the structure of **2**, two unique 4,4'-bipyridyl molecules are found, one of which coordinates to the nickel center via its nitrogen atoms, whereas the other is involved only in hydrogen bonded linkage. Both types of 4,4'-bipyridyl units are nonplanar, having torsional twists about their central linking bonds of ca. 16.3° and 43.1°, respectively. Notably, the non-coordinated 4,4'-bipyridyl guest is positioned over a crystallographic inversion center, and

Table 4
Hydrogen bonds exhibited by **1** and **2**

D–H	d(D–H)	d(H···A)	∠D–H···A	d(D···A)	A [symmetry]
Complex 1					
O33–H33	0.93(4)	1.66(4)	175(4)	2.586(3)	O22 [x,y,z]
O1–H1B	0.78(4)	1.98(4)	179(4)	2.767(2)	N11 [−x+3/2, y+1/2, −z+1/2]
O1–H1A	0.86(3)	1.84(4)	158(3)	2.660(2)	O22 [−x+1, −y, −z]
Complex 2					
O3–H3A	0.85	1.964	167.30(1)	2.799	N3 [x−1/2, y, −z+1]
O3–H3B	0.85	1.82	164.76(1)	2.65	O2 [−x+1/2, −y, +z]
C5–H5	0.93	2.514	178.34(1)	3.444	O2 [−x+1, −y, −z+1]
C21–H21	0.93	2.299	163.25(1)	3.201	O1 [x+1/2, y, −z+1]

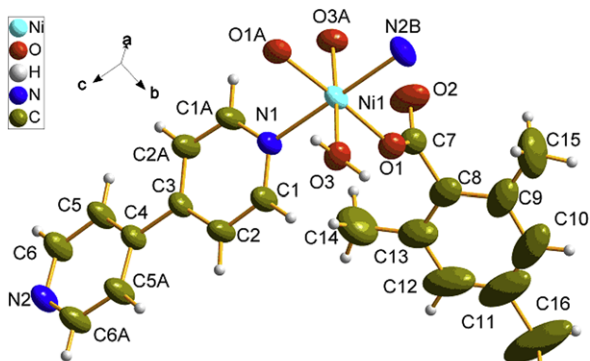


Fig. 4. A molecular diagram showing the coordination geometry of Ni^{II} in **2**. Symmetry codes (A) $-x+1/2, -y, z$; (B) $-x+1/2, y, z-1/2$.

therefore, there is a statistical reversal of the N–N axis throughout the structure, which however does not change the crosslinking hydrogen bonding role of it.

The least square plane calculations show that the dihedral angle between the phenyl rings of two 2,4,6-trimethylbenzoate anions is 8.32° for the planes containing (C8, C9, C10, C11, C12, and C13) and (C8a, C9a, C10a, C11a, C12a, and C13a), and the dihedral angle between the two 4,4'-bipyridyl units is 73.51° for the planes containing (N1, C1–C6, N2, and C1'–C6') and (N1a, C1a–C6a, N2a, and C1a'–C6a'), and the dihedral angle between the 4,4'-bipyridyl ring and a phenyl ring of 2,4,6-trimethyl benzoate anion is 48.41° for the planes containing (C8, C9, C10, C11, C12 and C13) and (N1, C1–C6, N2 and C1'–C6').

The bond lengths involving 4,4'-bipyridyl and 2,4,6-trimethyl benzoate ligands are Ni–O(carboxyl) [2.042(1) Å], Ni–O(water) [2.0084(1) Å], and Ni–N [2.104(1) and 2.105(2) Å], being virtually similar to the mean database values for these bonds [2.061, 2.087, and 2.103 Å, respectively]. The O–Ni–O angles are in the

range of 89.54(5)–177.55(7) with the average value of 118.99° and the O–C–O angle is 125.32(18)°.

Each coordinated water molecule provides one H atom to the coordinating carboxylate O atom and the other to the N atom of uncoordinated 4,4'-bpy [$d_{O3-H3A \cdots N3} (x-1/2, y, -z+1) = 2.799(0)$ Å and $\angle = 167.30(1)^\circ$] and [$d_{O3-H3B \cdots O2} (-x+1/2, -y, z) = 2.650(0)$ Å and $\angle = 164.76(1)^\circ$]. The strong hydrogen bonds are apparently responsible for the supramolecular assembly of the 1D coordination chains to generate 3D networks. In fact, considering these H-bonds, each metal center behaves as a planar four-connected node to constitute 3D CdSO₄ topological frameworks [25], which are interestingly of 2-fold interpenetration in the crystalline lattice (see Figs. 6–8). Intermolecular C–H···O interactions [$d_{C5-H5 \cdots O2} (-x+1, -y, -z+1) = 3.444$ Å and $\angle = 178.34(1)^\circ$] and [$d_{C21-H21 \cdots O1} (x+1/2, y, -z+1) = 3.201$ Å and $\angle = 163.25(1)^\circ$] are also found, which play a significant role in stabilizing this structure. The vibrational frequencies [26] of **1** and **2** are given in Table 5.

3.3. Magnetic properties

Temperature-dependent magnetic susceptibility measurements for complexes **1** and **2** were performed on polycrystalline samples. The effective magnetic moments of **1** and **2** are 5.68 and 3.42 μ_B , being close to the expected values (5.2 and 3.9 μ_B) for the isolated high-spin Co(II) and Ni(II) ($S = 5/2$). A χ_M versus T plot for **1** over the temperature range of 23.7–291.8 K (Fig. 9), in which χ_M is the corrected magnetic susceptibility per Co(II) unit, could be fitted according to the Curie–Weiss law $\chi_M = C/(T - \theta)$, giving a Curie constant $C = 4.03$ cm³ mol^{−1} K, and a Weiss constant $\theta = -22.51$ K. The negative value of θ indicates weak antiferromagnetic interactions between Co(II), since the adjacent Co(II) ions are separated with distance of 13.022 Å as revealed by X-ray crystal structure. The χ_M value of 1.2×10^{-2} cm³ mol^{−1} at room temperature increases as the temperature decreases, attaining 9.8×10^{-2} cm³ mol^{−1} at 23.7 K. A χ_M versus T plot for **2** over the temperature range of 8.4–296.7 K (Fig. 10), in which χ_M is the corrected magnetic susceptibility per Ni(II) unit, could be fitted according to the Curie–Weiss law $\chi_M = C/(T - \theta)$, giving a Curie constant $C = 1.46$ cm³ mol^{−1} K, and a Weiss constant $\theta = -34.92$ K. Similarly, the negative value of θ indicates antiferromagnetic interactions between Ni(II), since the adjacent Ni(II) ions are separated by 4,4'-bpy ligands with distance of 11.3 Å. The χ_M value of 4.91×10^{-3} cm³ mol^{−1} at room temperature increases as the temperature decreases, attaining 6.8×10^{-2} cm³ mol^{−1} at 8.4 K.

3.4. Thermal properties

Thermal analysis (TGA) of complexes **1** and **2** were performed between room temperature and 700°C under the nitrogen atmo-

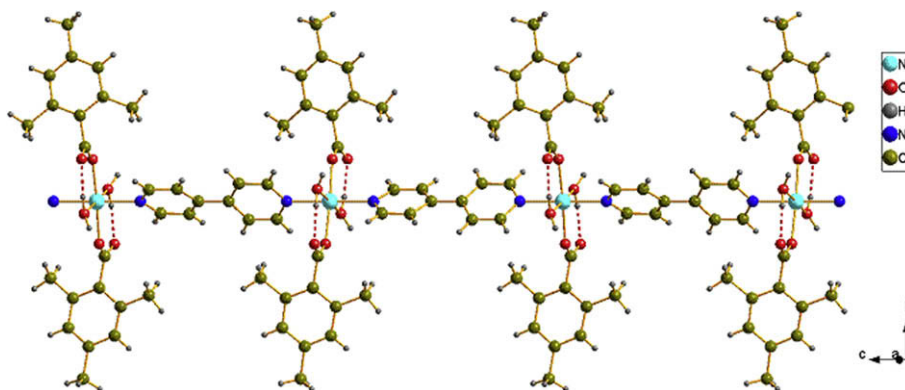


Fig. 5. The polymeric single chain in **2**.

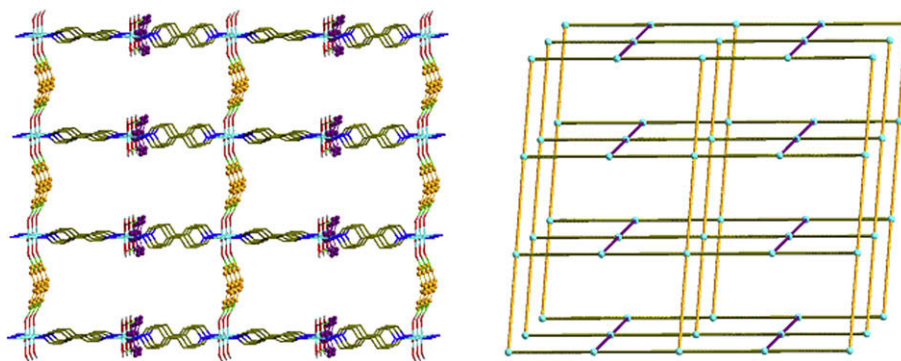


Fig. 6. A single 3D network in **2** (left). A schematic representation of the cds (CdSO_4) topology (right). The 4,4'-bipy molecules involving in H-bonds are shown in violet and orange, respectively, and the 2,4,6-trimethyl benzencarboxylic acid ligands are omitted for clarity. (For interpretation of the references to colour in this figure legend, the reader is referred to the web version of this article.)

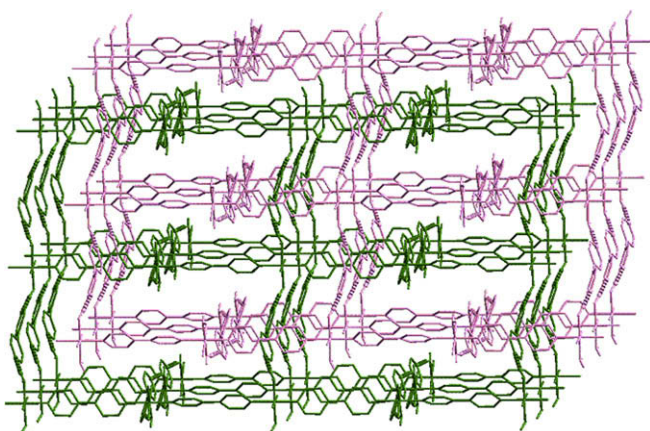


Fig. 7. 2-Fold interpenetrating structure of **2**. The two cds arrays are shown in green and rose, respectively. (For interpretation of the references to colour in this figure legend, the reader is referred to the web version of this article.)

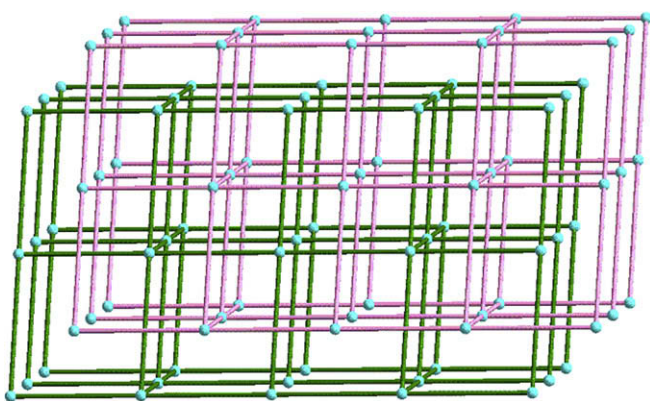


Fig. 8. A schematic view of two interpenetrating networks.

sphere. The TGA results indicate that **1** undergoes a weight loss of 3.7% (Calc. 3.3%) in the temperature range of 85–106 °C, corresponding to the removal of two coordinated water molecules. The second stage has the weight loss of 52.2% (Calc. 51.5%) in the temperature range of 146–274 °C, corresponding to removal of two 4,4'-bpy moieties and an unligated Htmb. The third stage occurs with the gradual decomposition of the remaining species, leading to the formation of cobalt oxide. The saturation temperature above which there is no obvious weight loss occurs at ~425 °C.

The TGA results indicate that complex **2** loses 5.1% (Calc. 4.9%) of its mass in the temperature range of 92–108 °C, corresponding

Table 5
Infrared spectral data of **1** and **2**

Frequency range (cm^{-1})		Mode of vibration
Compound 1	Compound 2	
3388	3415	O–H _{str} (water)
	3133	inter molecular H-bonding
3059	3061	aromatic C–H _{str}
2919 and 2857	2929 and 2863	aliphatic C–H _{str}
1604 and 1544	1609 and 1531	COO ⁻ asymmetric and COO ⁻ symmetric stretching [26]
1439–1004	1450–946	C=C and C–N stretching vibrations
764 and 806	754 and 846	C–H out of plane bending
Below 600	below 600	M–N and M–O stretching vibrations

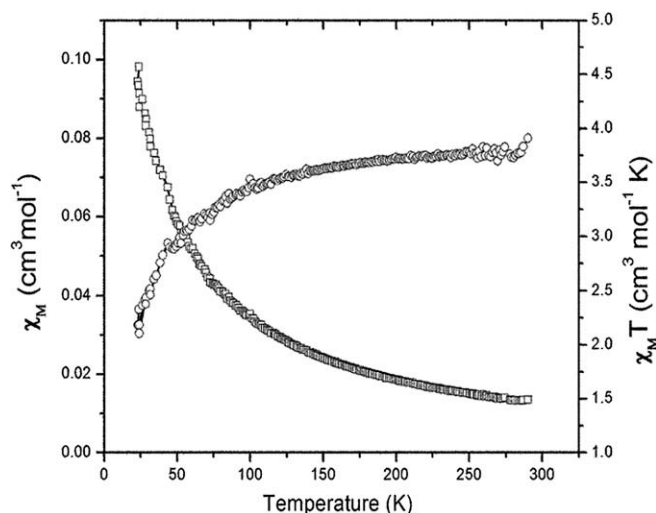


Fig. 9. χ_M and $\chi_M T$ vs. T plots for complex **1**. The solid lines represent the best fit of the experimental data.

to the loss of coordinated water molecules. The second stage involves the loss of 85.7% (Calc. 87.0%) of its mass in the temperature range of 290–395 °C, corresponding to the loss of two 4,4'-bpy and two tmb components. The third stage occurs with the gradual decomposition of the remaining species, leading to the formation of nickel oxide. The saturation temperature above which there is no obvious weight loss occurs at ~530 °C.

3.5. Electronic absorption spectra

In the electronic spectrum for complex **1**, the ligand 4,4'-bipyridyl exhibits a low energy band at 320 nm region, which is gener-

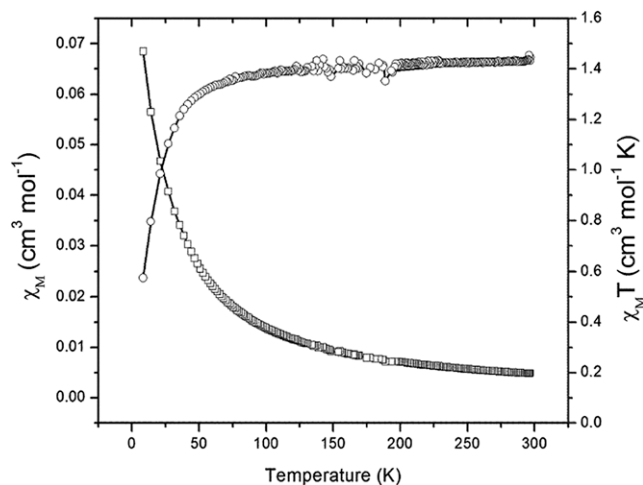


Fig. 10. χ_M and $\chi_M T$ vs. T plots for complex **2**. The solid lines represent the best fit of the experimental data.

ally assigned to π - π^* transition of the benzenoid and/or (C=N) chromophore of the ligand. As a rule, the longer wavelength bands in the spectra of metal complexes may be considered as evidence for the complex formation. The absorption band at 535 nm due to the ${}^4T_{1g} \rightarrow {}^4T_{1g}$ (P) transition, suggests a high-spin octahedral sphere. However, the presence of an additional absorption band as a shoulder in the 680 nm region, assigned to the ${}^4T_{1g} \rightarrow {}^4A_{2g}$ transition, suggests a distorted-octahedral configuration due to the Jahn–Teller effect.

The electronic spectrum of the Ni(II) complex **2** shows two absorption bands at 390 and 700 nm due to the MLCT transitions, as generally observed for octahedral Ni(II) complexes.

3.6. Antibacterial and antifungal activity

The *in vitro* biological screening effects of both complexes were tested against the bacteria: *Escherichia coli*, *Staphylococcus aureus*, *Pseudomonas aeruginosa*, and *Bacillus subtilis* by the well-diffusion method [27] using agar nutrient as the medium. The antifungal activities were also evaluated by the well-diffusion method against the fungi viz., *Aspergillus niger*, *Aspergillus flavus* and *Rhizoctonia bataicola* cultured on potato dextrose agar as medium. The compounds were tested at a concentration of 50 $\mu\text{g}/0.01$ mL in aqueous solution. In a typical procedure [28], a well was made on the agar medium inoculated with microorganisms. The well was filled with the test solution using a micropipette and the plate was incubated for 24 h for bacteria and 72 h for fungi at 35 °C. During this period, the test solution diffused and the growth of the inoculated microorganisms was affected. The inhibition zone was developed, at which the concentration was noted. The percentage inhibition was calculated as $100(C - T)/C$, where C is the average diameter of bacteria or fungal growth on the control plate (water) and T is the average diameter of bacteria or fungal growth on the test plate.

The susceptibility zones were measured in diameter (mm) and the results are shown in Tables 6 and 7. The susceptibility zones measured are the clear zones around the discs killing the bacteria. The complexes individually exhibit varying degrees of inhibitory effect on the growth of the tested bacterial species. On complexation, the polarity of the metal ion will be reduced to a greater extent due to the overlap of the ligand orbital and partial sharing of the positive charge of the metal ion with the donor groups. Further, it increases the delocalization of π -electrons over the whole ligand and enhances the penetration of complexes into lipid membranes and blocking of the metal binding sites in the enzymes of

Table 6
Antibacterial activity of the complexes **1** and **2**

Complex	Bacterial species				
	a	b	c	d	e
$[\text{Co}(\text{tmb})_2(4,4'\text{-bpy})_2](\text{Htmb})_2$	+++	++	++	+++	+++
$[\text{Ni}(\text{tmb})_2(\mu\text{-}4,4'\text{-bpy})(\text{H}_2\text{O})_2]_n(4,4'\text{-bpy})$	+++	++	++	+++	+++

a: *Escherichia coli*, b: *Staphylococcus aureus*, c: *Pseudomonas aeruginosa*, d: *Bacillus subtilis*; e: *Klebsiella pneumoniae*. Inhibition zone diameter mm (% inhibition): +, 6–10 (27–45%); ++, 10–14 (45–64%); +++, 14–18 (64–82%); +++, 18–22 (82–100%). Percent inhibition values were relative to inhibition zone (22 mm) of standard antibacterials (sulfadiazine, sulfathiazole), considered as 100% inhibition, tested under the same conditions as the new compounds reported here.

Table 7
Antifungal activity of the complexes **1** and **2**

Complex	Fungal species		
	a	b	c
$[\text{Co}(\text{tmb})_2(\text{bpy})_2](\text{Htmb})_2$	+++	++	++
$[\text{Ni}(\text{tmb})_2(\mu\text{-}4,4'\text{-bpy})(\text{H}_2\text{O})_2]_n(4,4'\text{-bpy})$	+++	++	++

a: *Aspergillus niger*, b: *Aspergillus flavus*, c: *Rhizoctonia bataicola*. Inhibition zone diameter mm (% inhibition): +, 6–10 (27–45%); ++, 10–14 (45–64%); +++, 14–18 (64–82%); +++, 18–20 (82–100%), (–) = no inhibition zone. Percent inhibition values were relative to inhibition zone (20 mm) of standard antifungal (Bavistin), considered as 100% inhibition, tested under the same conditions as the new compounds reported here.

microorganisms. The complexes may also disturb the respiration process of the cell and thus block the synthesis of proteins, which restricts further growth of the organism [29].

4. Conclusion

In summary, two new supramolecular complexes of Co^{II} and Ni^{II} using 2,4,6-trimethyl benzoic acid and 4,4'-bipyridyl as ligands have been synthesized by hydrothermal reaction and characterized by X-ray crystallography, IR, UV/Vis spectra, elemental analysis and magnetic susceptibility measurements. Both complexes display interesting 3D hydrogen-bonded assemblies from the fundamental discrete or 1D coordination arrays. Weak intermolecular antiferromagnetic interactions are found in **1** and **2**, which also show good antibacterial and antifungal activity.

Acknowledgement

The authors (MI and RR) acknowledge CSIR, New Delhi for providing financial support through Senior Research Fellowship. The authors greatly acknowledge Dr. H.N. Vasan, Principal Research Scientist, SSCU, Indian Institute of Science, Bangalore-12 for his constant encouragement and moral support. M.D. also acknowledges the financial support from Tianjin Normal University.

Appendix A. Supplementary data

CCDC 680843 and 680844 contain the supplementary crystallographic data for this paper. These data can be obtained free of charge via <http://www.ccdc.cam.ac.uk/conts/retrieving.html>, or from the Cambridge Crystallographic Data Centre, 12 Union Road, Cambridge CB2 1EZ, UK; fax: (+44) 1223-336-033; or e-mail: deposit@ccdc.cam.ac.uk. Supplementary data associated with this article can be found, in the online version, at [doi:10.1016/j.poly.2008.09.003](https://doi.org/10.1016/j.poly.2008.09.003).

References

- [1] S. Kitagawa, R. Kitaura, S. Noro, *Angew. Chem., Int. Ed.* 43 (2004) 2334.
- [2] F. Mori, T. Nyui, T. Ishida, T. Nogami, K. Ychoi, H. Nojiri, *J. Am. Chem. Soc.* 128 (2006) 1440.
- [3] B. Zhao, X.Y. Chen, P. Cheng, D.Z. Liao, S.P. Yan, Z.H. Jiang, *J. Am. Chem. Soc.* 126 (2004) 15394.
- [4] A. Cingolani, S. Galli, N. Masciocchi, L. Pandolfo, C. Pettinari, A. Siroin, *J. Am. Chem. Soc.* 127 (2005) 6144.
- [5] (a) C.M. Liu, D.Q. Zhang, J.L. Luo, N.L. Wang, H.M. Hu, D.B. Zhu, *Eur. J. Inorg. Chem.* (2003) 3618;
(b) M. Kondo, T. Okubo, A. Asami, S. Noro, T. Yoshitomi, S. Kitagawa, T. Ishii, H. Matsuzaka, K. Seki, *Angew. Chem., Int. Ed.* 38 (1999) 140;
(c) L. Mao, S.J. Rettig, R.C. Thompson, J. Trotter, S.-H. Xia, *Can. J. Chem.* 74 (1996) 2413;
(d) S.K. Ghosh, P.K. Bharadwaj, *Inorg. Chem.* 43 (2004) 6887;
(e) S.K. Ghosh, P.K. Bharadwaj, *Eur. J. Inorg. Chem.* (2005) 4880;
(f) Y. Liang, R. Cao, W.P. Zhu, M.C. Hong, W.J. Zhang, *Angew. Chem., Int. Ed.* 39 (2000) 3304;
(g) Y. Liang, M.C. Hong, W.P. Zhu, R. Cao, W.J. Zhang, *Inorg. Chem.* 40 (2001) 4574.
- [6] M.J. Zaworotko, *Chem. Commun.* (2001) 1.
- [7] S.R. Batten, R. Robson, *Angew. Chem., Int. Ed.* 37 (1998) 1460.
- [8] M.L. Tong, H.K. Lee, X.M. Chen, R.B. Huang, T.C.W. Mak, *J. Chem. Soc., Dalton Trans.* (1999) 3657.
- [9] M. Andruh, H.W. Roesky, M. Noltemeyer, H.G. Schmidt, *Z. Naturforsch., Teil. B* B49 (1994) 31.
- [10] K. Biradha, M. Fujita, *Chem. Commun.* (2001) 15.
- [11] Q. Wang, X. Wu, W. Zhang, T. Sheng, P. Lin, J. Li, *Inorg. Chem.* 38 (1999) 2223.
- [12] K. Biradha, M. Sarkar, L. Rajput, *Chem. Commun.* (2006) 4169.
- [13] B.F. Hoskins, P.J. Oliver, G. Winter, *Inorg. Chim. Acta* 86 (1984) L21.
- [14] C.L. Ma, J.K. Li, R.F. Zhang, D.Q. Wang, *Inorg. Chim. Acta* 359 (2006) 2407.
- [15] G.M. Sheldrick, *SHELXL97* and *SHELXS97*, University of Göttingen, Germany, 1997.
- [16] L.J. Farrugia, *J. Appl. Crystallogr.* 30 (1997) 565.
- [17] *SADABS*, Empirical Absorption Correction Program, University of Göttingen, Göttingen, Germany, 1997.
- [18] G.M. Sheldrick, *SAINT*, 5.1 ed., Siemens Industrial Automation Inc., Madison, WI, 1995.
- [19] G.M. Sheldrick, *SHELXTL Reference Manual: Version 5.1*; Bruker AXS: Madison, WI, 1997.
- [20] Y. Sun, Z. Wang, H. Zhang, Y. Cao, S. Zhang, Y. Chen, C. Huang, X. Yu, *Inorg. Chim. Acta* 360 (2007) 2565.
- [21] Y.-H. Liu, Y.-L. Lu, H.-L. Tsai, J.-C. Wang, K.-L. Lu, *J. Solid State Chem.* 158 (2001) 315.
- [22] F. Jin, J. Li, H. Zhou, J. Wu, J. Yang, Y. Tian, M. Jiang, *J. Mol. Struct.* 829 (2007) 202.
- [23] J.C.A. Boeyens, *J. Cryst. Mol. Struct.* 8 (1978) 317.
- [24] D. Cremer, J.A. Pople, *J. Am. Chem. Soc.* 97 (1975) 1354.
- [25] D.M.L. Goodgame, D.A. Grachvogel, A.J.P. White, D.J. Williams, *Inorg. Chem.* 40 (2001) 6180.
- [26] K. Nakamoto, *Infrared and Raman Spectra of Inorganic and Coordination Compounds*, Fourth ed., Wiley, New York, 1986.
- [27] C. Perez, M. Pauli, P. Bazerque, *Acad Biol. Et. Med. Exp.* 15 (1990) 113.
- [28] M.J. Pelczar, E.C.S. Chan, N.R. Krieg, *Microbiology*, fifth ed., Blackwell, Science, New York, 1998.
- [29] N. Dharmaraj, P. Viswanathamurthi, K. Natarajan, *Transition Met. Chem.* 26 (2001) 105.